Reshaping the Jaynes-Cummings ladder with Majorana bound states

L. S. Ricco [1,*] V. K. Kozin,[1,2] A. C. Seridonio,[3] and I. A. Shelykh[1,4]
[1] *Science Institute, University of Iceland, Dunhagi-3, IS-107 Reykjavik, Iceland*
[2] *Department of Physics, University of Basel, Klingelbergstrasse 82, CH-4056 Basel, Switzerland*
[3] *School of Engineering, Department of Physics and Chemistry, São Paulo State University (UNESP), 15385-000 Ilha Solteira, São Paulo, Brazil*
[4] *Department of Physics, ITMO University, St. Petersburg 197101, Russia*

(Received 30 March 2022; revised 9 June 2022; accepted 18 July 2022; published 2 August 2022)

We study the optical properties of a hybrid device composed by a quantum dot (QD) resonantly coupled to a photonic mode of an optical microcavity and a Majorana nanowire: a topological superconducting segment hosting Majorana bound states (MBSs) at the opposite ends. In the regime of strong light-matter coupling, it is demonstrated that the leakage of the Majorana mode into the QD opens new optical transitions between polaritonic states formed due to hybridization of material excitation with cavity photons, which leads to the reshaping of the Jaynes-Cummings ladder and can lead to the formation of a robust single peak at cavity eigenfrequency in the emission spectrum. Moreover, weak satellite peaks in the low- and high-frequency regions are revealed for the distinct cases of highly isolated MBSs, overlapped MBSs, and MBSs not well localized at the nanowire ends.

DOI: 10.1103/PhysRevA.106.023702

I. INTRODUCTION

Almost a century ago, Majorana discovered the representation of the Dirac equation having real wavefunctions as its solutions [1]. They describe exotic particles which are equivalent to their own antiparticles, known as Majorana fermions. In the last years, the Majorana proposal attracted the continuous attention of the researchers outside the high-energy physics community, once it was shown that Majorana quasiparticles can emerge in condensed matter systems [2–6]. These Majorana-like excitations arise in topologically protected phases of matter [4] and possess exotic non-Abelian statistics [7]. Besides the interest from the fundamental viewpoint, the remarkable features of the Majorana quasiparticles make them attractive potential candidates for performing decoherence-free quantum computing operations [8,9].

Among several platforms where Majorana quasiparticles can emerge [2,5], one-dimensional hybrid semiconducting nanowires with strong Rashba spin-orbit interaction placed in contact with a superconductor [10–13] have been considered one of the best options. Under application of an external magnetic field, these so-called Majorana nanowires undergo the topological phase transition, characterized by the emergence of a p-wave superconducting gap supporting zero-energy Majorana bound states (MBSs) at the opposite ends of the proximitized nanowire [10].

One of the signatures of the formation of topologically protected MBSs at the ends of a Majorana nanowire is the emergence of a quantized zero-bias conductance peak (ZBCP) in tunneling conductance through a nanowire at very low temperatures [14–20], which is robust to variations of the system parameters, such as gate voltages and magnetic fields. In the corresponding geometry, a quantum dot (QD) side-coupled to a Majorana nanowire has been employed as a tunneling spectroscopic tool to probe MBSs and also measure the so-called degree of Majorana nonlocality [19,21–27].

While tunneling spectroscopic properties of hybrid QD-Majorana nanowires have been extensively studied over the last years, their optical properties did not attract any substantial attention, although some works in this field have started to appear [28–39]. On the other hand, individual QDs are widely applied in optical quantum information processing, where they can be used as a solid-state source of single photons [40], entangled photon pairs on demand [41–43], and other types of nonclassical light [44–46], as well as quantum filters [47–49] and other building blocks of quantum integrated photonic circuits [50–52].

In this context, a system consisting of a QD embedded inside a photonic cavity is of particular interest. If the cavity has a high quality factor and the excitonic transition in the dot is brought in resonance with the photonic eigenfrequency, the system enables a dramatic enhancement of the light-matter interaction. In this situation, the regime of strong light-matter coupling is achieved [53–55], and light and matter quantum states become hybridized. The energy spectrum is dramatically reshaped, and the so-called Jaynes-Cummings ladder emerges [56–58]. Its formation changes the emission spectrum, which for a symmetric QD evolves from the Rabi doublet to a Mollow triplet [59] with increase of the pump intensity, both for resonant and nonresonant pumping schemes [60–62]. Incorporation of the spatial inversion asymmetry into the quantum system further changes the emission pattern and leads to the opening of optical transitions at the

*Corresponding author: lsricco@hi.is

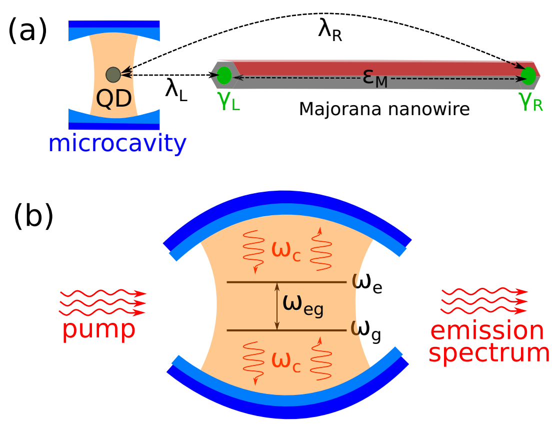

FIG. 1. (a) The sketch of the proposed device: a quantum dot (QD) embedded in an optical microcavity and coupled to a Majorana nanowire hosting Majorana bound states (MBSs) at its opposite ends (light green circles). λ_L and λ_R represent the couplings between the QD excited level and the left (γ_L) and right MBSs (γ_R), respectively, while ε_M stands for the overlap amplitude between the MBSs. (b) Optical transitions for a QD placed inside an optical microcavity. The dot interacts resonantly with a single-mode photonic field of the pumped cavity with frequency $\omega_c = \omega_{eg} = \omega_e - \omega_g$ brought in resonance with the energy of the optical transition, where ω_e and ω_g stand for the energies of the excited and ground states of the QD, respectively.

Rabi frequency which were forbidden in the symmetric case [63,64]. As well, transition from the case of small dots, where material excitations are fermionlike, to large quantum dots, when excitons behave more as bosons, is also associated with restructuring of the emission spectrum, which starts to reveal a complex multiplet structure [65,66].

In the present work, we explore the effects of the coupling between a Majorana nanowire and a QD embedded in a microcavity (Fig. 1) in the regime of strong light-matter coupling, with the excitonic transition in the dot brought in resonance with the cavity eigenfrequency. It is demonstrated that the leakage of the MBS into the QD opens new optical transitions between the polaritonic states of the QD-microcavity system, which were originally forbidden in the absence of the Majorana nanowire. More specifically, the opening of these transitions is allowed due to the reshaping of the primary Jaynes-Cummings ladder due to the QD-Majorana nanowire finite coupling. The spatial position of the MBSs with respect to the nanowire ends, as well as the overlap between each other, directly affect the way in which the ladder rungs are reshaped. The emission spectrum is strongly modified due to the coupling between the QD and Majorana nanowire, showing a prominent single peak at the cavity eigenfrequency.

The paper is organized as follows. In Sec. II A, the model Hamiltonian is introduced. In Sec. II B, the theory describing the optical transitions and emission spectrum is presented. In Sec. III, we show the numerical results for the new optical transitions and corresponding emission spectrum for the cases of highly isolated and overlapped MBSs. The main results are summarized in Sec. IV.

II. MODEL AND METHODS

A. The Hamiltonian

We consider the system schematically shown in Fig. 1(a). A two-level QD, with the ground state $|g\rangle$ and the excited state $|e\rangle$, is embedded inside a single-mode cavity with frequency ω_c. In the absence of interaction, the ground state of the QD corresponds to the case with one electron in the lowest level and no electrons in the excited level of the QD, i.e, $|g\rangle \equiv |1, 0\rangle$, while the excited state is the opposite: $|e\rangle \equiv |0, 1\rangle$. The QD interacts resonantly with the cavity photonic field tuned at the frequency $\omega_c = \omega_{eg} = \omega_e - \omega_g$, where ω_e and ω_g are the energies of the excited and ground states of the dot, respectively [see Fig. 1(b)]. The QD excited level is coupled to both MBSs at opposite ends of a superconducting nanowire in the topological phase. The full Hamiltonian which describes the system reads

$$\hat{\mathcal{H}} = \hat{\mathcal{H}}_{JC} + \hat{\mathcal{H}}_M, \tag{1}$$

where

$$\begin{aligned}\hat{\mathcal{H}}_{JC} &= \omega_c a^\dagger a + \omega_e d_e^\dagger d_e + \omega_g d_g^\dagger d_g \\ &\quad + \Omega_R (d_g^\dagger d_e a^\dagger + d_e^\dagger d_g a)\end{aligned} \tag{2}$$

is the well-known Jaynes-Cummings (JC) model, describing optical transitions in the dot within the rotating wave approximation (RWA) [56,57] ($\hbar = 1$). The bosonic operator $a^\dagger$ (a) creates (annihilates) the cavity photons and $d_j^\dagger$ (d_j) creates (annihilates) an electron in the QD j level, where $j = e, g$. The last term on the right-hand side of Eq. (2) describes the coupling between the cavity photons and an electron in the QD, with the coupling strength Ω_R (Rabi frequency). It depends on the dipole matrix element of the optical transition and the cavity geometry.

The Hamiltonian which describes the topological superconducting nanowire (Majorana nanowire) side-coupled to the excited QD state reads [21,23,26,37,67]

$$\begin{aligned}\hat{\mathcal{H}}_M &= \imath \varepsilon_M \gamma_L \gamma_R + \lambda_L (d_e - d_e^\dagger) \gamma_L \\ &\quad + \lambda_R (d_e + d_e^\dagger) \gamma_R,\end{aligned} \tag{3}$$

where the operators γ_L and γ_R represent the MBSs at the left and right ends of the Majorana nanowire, respectively, with $\gamma_a = \gamma_a^\dagger$ [4], obeying the anticommutation relation $\{\gamma_a, \gamma_b\} = 2\delta_{a,b}$ ($a, b = L, R$). The overlap strength between the MBSs is given by ε_M, and λ_L and λ_R are the couplings between the electron at the QD excited level and left and right MBSs, respectively.

The effective Hamiltonian of Eq. (3) has been widely used in previous works [21–23,37,67], and allows us to explore the following situations.

(i) Highly isolated MBSs: This case corresponds to disorder-free and longer nanowires [68,69], where the topologically protected MBSs are well localized at the opposite ends of the nanowire ($\lambda_R = 0$) and do not overlap with each other ($\varepsilon_M = 0$) [70].

(ii) MBSs localized at the nanowire ends, but with overlap between them: As in the former case, the wavefunctions which describe the left and right MBSs are centered at the corresponding nanowire ends ($\lambda_R = 0$). However, due to a shorter nanowire length these wavefunctions strongly overlap with each other ($\varepsilon_M \neq 0$) [17,70].

(iii) Right MBS shifted from its nanowire end: Distinct from previous situations, now the wavefunction of the right MBS is not centered at its corresponding nanowire end, leading to a coupling with the QD ($\lambda_R \neq 0$, $\lambda_R \gg \varepsilon_M$) [22,23]. This case qualitatively emulates MBSs with partial spatial separation between them, which can appear due to inhomogeneous potentials in the nanowire [24,71]. Moreover, the finite value of λ_R is associated with the degree of Majorana nonlocality [23,37], also known as the topological quality factor [25,26].

It is worth emphasizing that the changing of the QD-MBS couplings λ_L and λ_R, as well as the MBS-MBS overlap ε_M, mimics realistic physical situations, as described above. Moreover, such quantities depend on external tunable parameters, such as the Majorana nanowire chemical potential and the magnetic field strength applied perpendicularly to the nanowire [23,70,72], for instance.

It is convenient to write $\hat{\mathcal{H}}_M$ [Eq. (3)] in terms of canonical fermion operators c_M, which obey usual anticommutation relations for fermions, $\{c_M, c_M^\dagger\} = 1$ and $\{c_M, c_M\} = \{c_M^\dagger, c_M^\dagger\} = 0$. According to this representation, the Majorana operators are rewritten as [21,67,73] $\gamma_L = (c_M^\dagger + c_M)/\sqrt{2}$ and $\gamma_R = \imath(c_M^\dagger - c_M)/\sqrt{2}$, and thus $\hat{\mathcal{H}}_M$ becomes

$$\hat{\mathcal{H}}_M = \varepsilon_M n_M + \Lambda^-(d_e c_M^\dagger + c_M d_e^\dagger) + \Lambda^+(d_e c_M + c_M^\dagger d_e^\dagger), \tag{4}$$

with $n_M = c_M^\dagger c_M$ being the number operator associated to the fermionic operator given by the combination of the Majorana operators $\gamma_{L,R}$ and $\Lambda^\pm = (\lambda_L \pm \lambda_R)/\sqrt{2}$. Although c_M stands for a canonical operator, it has a nonlocal character, once it comes from the combination of two MBSs which are spatially far apart from each other.

It should be noted that, distinct from the case of the JC Hamiltonian [57,64], $[\hat{\mathcal{H}}, \hat{N}] \neq 0$, i.e., the system Hamiltonian of Eq. (1) does not commute with the excitation number operator

$$\hat{N} = a^\dagger a + d_e^\dagger d_e + c_M^\dagger c_M, \tag{5}$$

due to the presence of the term $\Lambda^+(d_e c_M + c_M^\dagger d_e^\dagger)$ in $\hat{\mathcal{H}}_M$ [Eq. (3)], indicating that the number of electron-photon excitations in the system is not conserved. This is a consequence of the superconducting nature of the Majorana nanowire, which does not conserve the number of excitations.

B. Optical transitions and emission spectrum

The interaction term of the JC Hamiltonian [last one on the right-hand side of Eq. (2)] corresponds to the process of transferring the electron from the ground state $|g\rangle$ to the excited state $|e\rangle$ or vice versa by absorbing or emitting one photon from or to the cavity, i.e, $|g, n\rangle \leftrightarrow |e, n-1\rangle$, with $|g(e), n\rangle = |g(e), n\rangle \otimes |n\rangle$. These processes result in the formation of hybridized states, describing the QD dressed by the cavity photons, known as upper (U) and lower (L) polaritons. If the cavity is tuned exactly in resonance with ground-to-excited state transitions, their wavefunctions are $|U, n\rangle = (|g, n\rangle + |e, n-1\rangle)/\sqrt{2}$, $|L, n\rangle = (|g, n\rangle - |e, n-1\rangle)/\sqrt{2}$. In the regime of strong light-matter coupling, the allowed optical transitions between the upper and lower polaritons due to either emission or absorption of a cavity photon gives rise to the so-called JC ladder [57,74].

The optical transitions between the eigenstates of Eq. (1) corresponding to different occupation numbers n of cavity photons can be computed by considering an exchange between the cavity photons of Fig. 1 and the "outside world" (the reservoir of modes outside the system). This exchange is possible due to both an external incoherent pump applied to the QD-microcavity system and due to photons being able to escape the microcavity due to its finite lifetime. The coupling between the closed system and the reservoir can be accounted for by the following Hamiltonian:

$$\hat{\mathcal{H}}_{ex} = \Gamma a b^\dagger + \text{H.c.}, \tag{6}$$

where $b^\dagger$ (b) creates (annihilates) a photon in the external reservoir and Γ is the constant system-reservoir coupling strength [64]. The transition probabilities corresponding to the emission of a photon from the cavity to an empty external reservoir are proportional to

$$I_{if} \sim |\langle \psi_{f,n}, 1_{out}|\hat{\mathcal{H}}_{ex}|\psi_{i,n}, 0_{out}\rangle|^2, \tag{7}$$

where $|\psi_{i,n}\rangle$ and $|\psi_{f,n}\rangle$ are initial and final eigenstates associated to the system Hamiltonian [Eq. (1)], and 0_{out} and 1_{out} represent the zero- and one-photon states of the reservoir. By substituting Eq. (6) into Eq. (7), we obtain

$$I_{if} \sim |\langle \psi_{f,n}|a|\psi_{i,n}\rangle|^2. \tag{8}$$

Although the analysis of the optical transitions through Eq. (8) is useful for discussing the opening of new transitions induced in the QD-microcavity system due to its coupling with the Majorana nanowire, it does not allow us to obtain the shape of the corresponding emission spectrum for a given incoherent pump and cavity photons lifetime.

The standard way of computing both the external incoherent pumping P and the decay of photons, γ_{ph}, from the closed system to the reservoir is obtaining the full density matrix ρ of the system through the master equation [74]

$$\partial_t \rho = -\frac{\imath}{\hbar}[\hat{\mathcal{H}}, \rho] + \mathcal{L}\rho, \tag{9}$$

where $\mathcal{L}$ is the Lindblad superoperator. By solving numerically Eq. (9), the density matrix in the steady-state (SS) regime, ρ^{SS}, can be found, which provides the information about the occupations of different quantum states of the system for a given P and γ_{ph}.

The emission spectrum in the SS regime can be numerically obtained by a modified Fermi golden rule [64] and reads

$$S(\omega) \sim \varrho(\omega) \sum_{i,f} \rho_{ii}^{\text{SS}} I_{if} \frac{\gamma_{\text{ph}}^2}{(\varepsilon_i - \varepsilon_f - \omega)^2 + \gamma_{\text{ph}}^2}, \tag{10}$$

wherein $\varrho(\omega) \propto \omega^3$ is the reservoir density of states, I_{if} [Eq. (8)] are the transition probabilities between the initial and final states of the system Hamiltonian associated with photon emission to the reservoir, with the corresponding eigenenergies $\varepsilon_{i,f}$, and ρ_{ii}^{SS} are probabilities to find the system in the

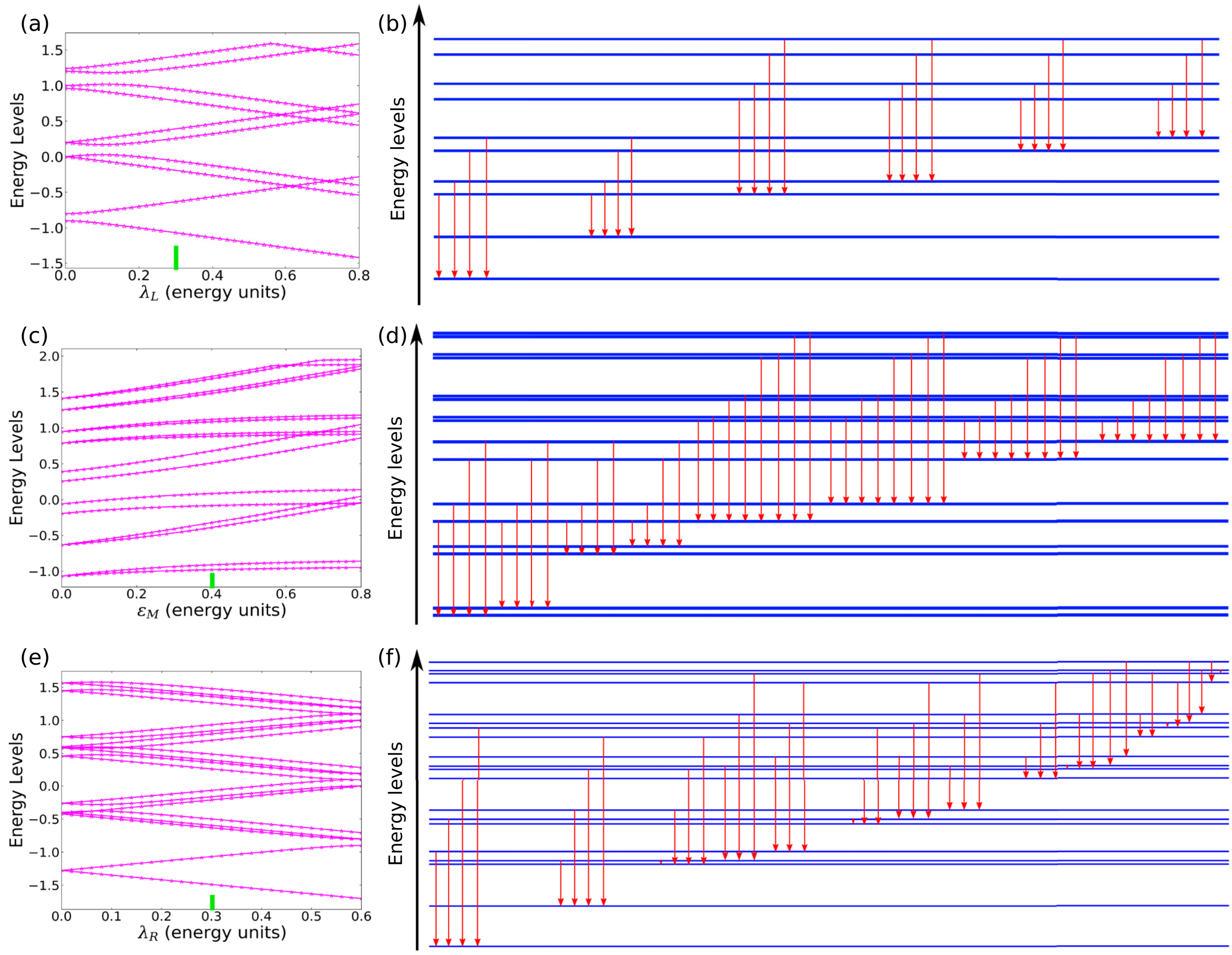

FIG. 2. Left: Evolution of the first 20 energy levels of the system as a function of the parameters of QD-MBS couplings λ_L and λ_R, as well as the overlap between the MBSs ε_M. Right: Optical transitions between the system eigenenergies for each corresponding case. The blue lines represent the initial and final states of each corresponding transition, which is represented by a red arrow. The specific parameters adopted in each of the right panels are indicated by the light green rectangle in the corresponding left ones. [(a), (b)] The case of well-isolated MBSs localized at the nanowire ends, with $\lambda_L = 0.3$ in (b). [(c), (d)] The situation of overlapped MBSs well localized at the nanowire ends, for $\lambda_L = 0.3$ and $\varepsilon_M = 0.4$ in (d). [(e), (f)] The case wherein the MBSs barely overlap, but are not well localized at the ends of the nanowire, with $\lambda_L = 0.6$ and $\lambda_R = 0.3$ in (f).

eigenstates of $\hat{\mathcal{H}}$ which should be obtained by solving master equation (9).

III. RESULTS AND DISCUSSION

Below, we numerically compute the optical transition probabilities [Eq. (8)] for a QD embedded in the microcavity and coupled to the Majorana nanowire ($\lambda_L \neq 0$), considering the cases (i), (ii), and (iii) previously discussed in Sec. II A. We set the following parameters for the QD embedded in the microcavity: energy of QD excited state, $\omega_e = 0.1$, energy of QD ground state, $\omega_g = -0.9$, Rabi frequency $\Omega_R = 0.1$, and eigenfrequency of the cavity photons, $\omega_c = \omega_e - \omega_g = 1.0$, all in energy arbitrary units. The numerical calculations were carried out using the QUTIP 4.6.2 package (PYTHON 3.8.10) [75,76]. Moreover, in all the results we use the distance between ground and excited states as an energy unit.

Figure 2 shows the allowed optical transitions, as well as the evolution of the first 20 eigenenergies of the Hamiltonian [Eq. (1)] for several values related to the QD-Majorana nanowire parameters λ_L, λ_R, and ε_M. The allowed transitions between the eigenenergies are represented by red arrows. Figure 2(a) specifically exhibits the behavior of the energy spectrum of the composite system (cavity photons–QD–Majorana nanowire) as the QD–left MBS coupling λ_L is increased, for the case wherein the MBSs are well localized at the nanowire ends, totally apart from each other [case (i)]. It can be easily seen that a finite λ_L leads to the appearance of new energy levels which are not present in the original JC ladder. Moreover, the energy levels which belong to the JC model are renormalized, leading to a shift in the original rungs of the JC ladder. This reshape of energy levels allows new optical transitions if compared to the allowed transitions in the JC model [57,64,74], as shown in Fig. 2(b) for $\lambda_L = 0.3$. It can be

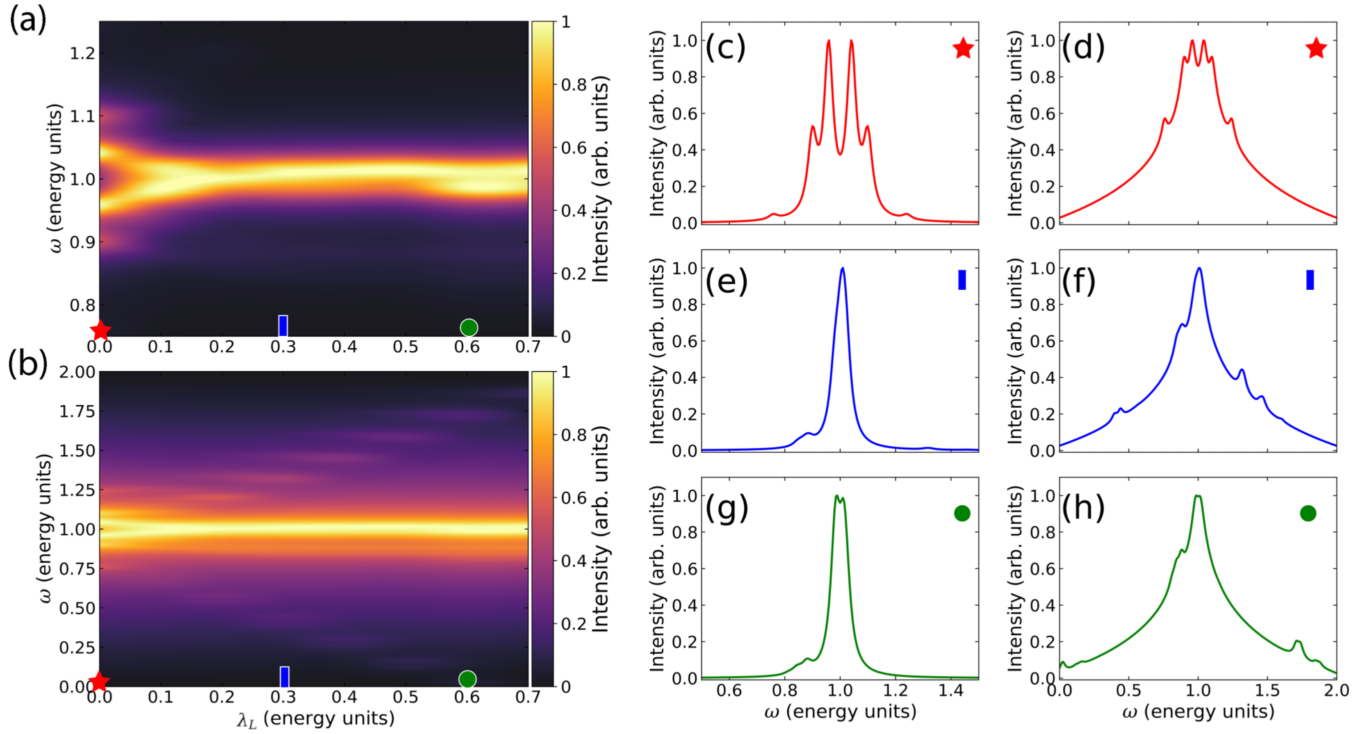

FIG. 3. Normalized emission spectrum [Eq. (10)] for the situation of isolated MBSs localized at opposite nanowire ends ($\lambda_R = \varepsilon_M = 0$), with $\omega_c = \omega_{eg} = 1.0$, $\Omega_R = 0.1$, $P = 0.015$, and $\gamma_{\rm ph} = 0.02$. [(a), (b)] Intensity of emission spectrum as a function of both emitted photon frequency ω and QD–left MBS coupling λ_L, in linear and logarithmic scales, respectively. [(c), (e), (g)] Linecuts indicated by geometric shape markers in (a); [(d), (f), (h)] the same linecuts, but in logarithmic scale.

noticed that there are transitions between two nearest energy levels and between two more distant levels. These transitions will be responsible for an emitted radiation in regions far from ω_c, as we see later on.

Figure 2(c) depicts the evolution of the system energy spectrum as the overlap strength ε_M between the MBSs bound at opposite ends of the Majorana nanowire is enhanced [case (ii)] (we keep $\lambda_L = 0.3$). It can be noticed that the effect of a finite ε_M is breaking the degeneracy of certain eigenenergies, which consequently leads to additional rungs in the ladder, if compared to Fig. 2(b). The reshape of the energy spectrum due to the overlap between left and right MBSs also allows new optical transitions between nearest and more distant rungs, as shown in Fig. 2(d), where $\varepsilon_M = 0.4$ [light green rectangle in Fig. 2(c)].

The case in which the right MBSs are not well localized at the right nanowire end [case (iii)], leading to a finite coupling with the QD ($\lambda_R \neq 0$), is illustrated in Fig. 2(e). The corresponding energy spectrum evolution for increasing values of λ_R, with $\lambda_L = 0.6$ and $\varepsilon_M = 10^{-3}$, reveals that the finite QD–right MBS hybridization also leads to a degeneracy breaking if compared to the case of isolated MBSs [Fig. 2(a)]. As in the previous case of overlapped MBSs [Fig. 2(d)], the emergence is observed in Fig. 2(f) of new rungs in the ladder, also allowing new optical transitions. But distinct from the overlapped case, the coupling between the QD and the right MBS opens transitions between extremely close ladder rungs, which will be responsible for near-zero-frequency peaks in the emission spectrum profile for any value of λ_R, as we see further on.

In the following figures, the emission spectrum [Eq. (10)] behavior is analyzed in detail for the same set of QD-microcavity parameters adopted in Fig. 2, considering the incoherent pumping intensity $P = 0.015$ and the cavity photon decay rate $\gamma_{ph} = 0.02$. For simplicity, we take the excitonic decay rate γ_{QD} to be zero. Notice that the regime of strong light-matter coupling $\Omega_R > |\gamma_{ph} - \gamma_{QD}|/4$ [74] is fulfilled.

The emission spectrum for the situation of isolated and well-localized MBSs at the nanowire ends [case (i)] is shown in Fig. 3. Figure 3(a) depicts the normalized emission spectrum as a function of both the QD–left MBS coupling λ_L and emitted photon frequency ω. For $\lambda_L = 0$ (red star marker), the emission spectrum shows a quadruplet pattern around the cavity photon eigenfrequency $\omega = \omega_c$, as shown in Fig. 3(c). This quadruplet structure is expected for the JC model in the strong-coupling regime in the presence of a small incoherent pump [64,77]. This multiplet structure, also known as a JC fork, is also shown on a logarithmic scale, as depicted in Figs. 3(b) and 3(d).

Figure 3(a) also reveals that as λ_L is increased, the multiplet structure coalesces into a single peak at $\omega = \omega_c$, with a smaller peak structure at $\omega \approx 0.9$. This is better seen in Fig. 3(e), which corresponds to $\lambda_L = 0.4$ [blue rectangle marker in Fig. 3(a)]. For bigger values of QD-left MBS coupling, the single-peak structure at $\omega = \omega_c$ undergoes a tiny splitting, but still preserves its single-peak shape, as shown in Fig. 3(g).

In addition to the evolution of the JC fork to a single peak shown in Fig. 3(a), the leakage of the isolated left MBS also

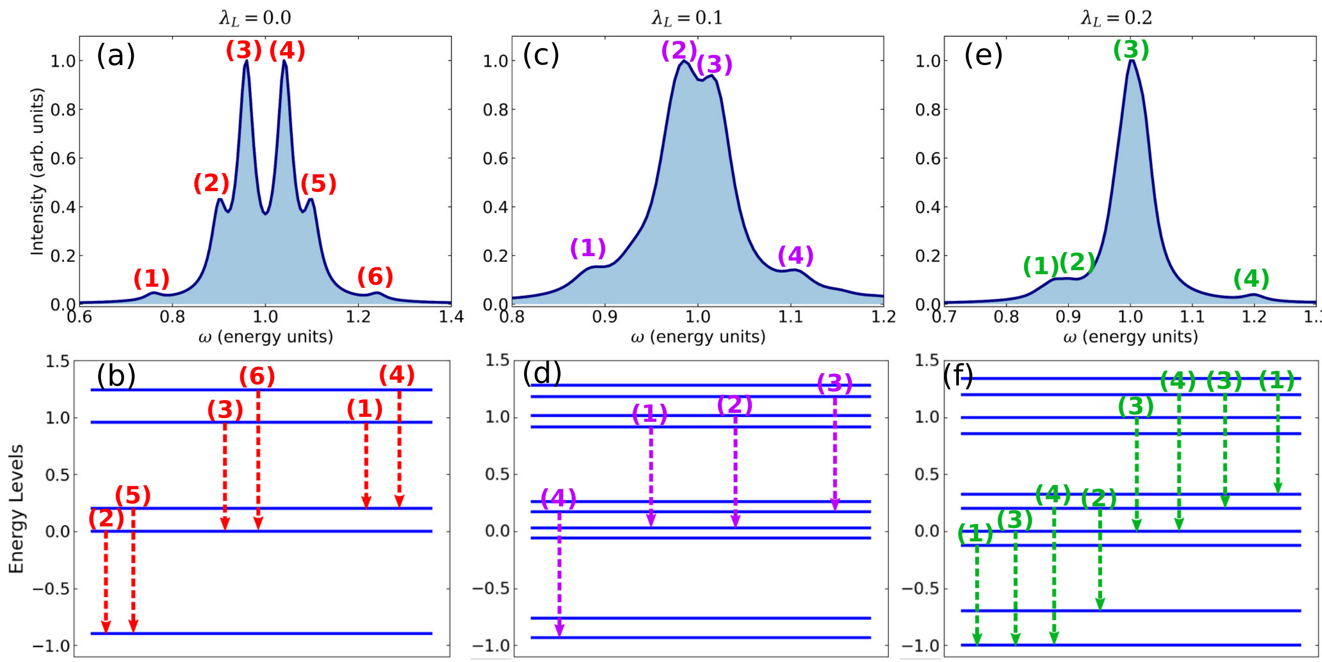

FIG. 4. Top: Normalized emission spectrum [Eq. (10)] as a function of the frequency of the emitted photon ω, for the situation in which the MBSs are well localized at the nanowire ends and do not overlap with each other ($\lambda_R = \varepsilon_M = 0.0$), with $\omega_c = \omega_{eg} = 1.0$, $\Omega_R = 0.1$, $P = 0.015$, and $\gamma_{\rm ph} = 0.02$, considering distinct values of the QD–left MBS coupling λ_L. Bottom: Allowed optical transitions of the system which correspond to the peaks in the top panels, labeled by colored numbers.

drives the formation of weaker peaks in the emission spectrum far from the cavity eigenfrequency region, which are visible only on a logarithmic scale, as depicted in Fig. 3(b) and the corresponding linecuts shown in Figs. 3(f)–3(h). Fig. 3(h), for instance, shows a finite emitted radiation at very low frequency ω close to the Rabi frequency, as well as some peaks near the double frequency $\omega = 2\omega_c$. The low-frequency signal can be amplified by placing the QD microcavity inside a terahertz-frequency cavity, which will resonantly enhance the density of states $\rho(\omega)$ and increase the emission up to a factor of 10 [78,79].

In Fig. 4, we investigate in detail the evolution of the normalized emission spectrum as a function of the emitted photon frequency ω, visible on a linear scale, and the corresponding optical transitions responsible for the emission spectrum peaks as λ_L is turned on, considering the same parameters adopted in Fig. 3. Figure 4(a) shows the emission spectrum when the QD-microcavity system is decoupled from the Majorana nanowire ($\lambda_L = 0$), wherein the well-known JC fork structure appears, with a well-resolved double peak around the cavity eigenfrequency $\omega_c = 1.0$. This multiplet profile comes from the JC ladder shown in Fig. 4(b) [64,77], in which each optical transition between the system eigenenergies corresponds to a peak in Fig. 4(a), as labeled by the red numbers.

Figure 4(c) depicts the emission spectrum for $\lambda_L = 0.1$. We can notice that the JC fork lineshape from Fig. 4(a) is deformed and the well-resolved peaks around $\omega = \omega_c$ become merged into each other. This changing in the emission spectrum profile comes from the emergence of new system eigenenergies or, equivalently, new rungs in the JC ladder, due to the leaking of the isolated left MBS into the QD, which opens new optical transitions, as depicted in Fig 4(d). The peaks in the emission spectrum around ω_c in Fig. 4(c), for instance, come from transitions (2) and (3) shown in Fig. 4(d).

For $\lambda_L = 0.2$, Fig. 4(e) shows that the JC fork structure is completely absent, with the appearance of a single peak at $\omega = \omega_c = 1.0$. This single peak indicates that optical transitions with the frequency on resonance with the cavity eigenfrequency are now allowed in the system. Particularly, these transitions are labeled by the green number (3) in Fig. 4(f) and the other optical transitions yield the satellite peaks in Fig. 4(e). In addition, comparison between Figs. 4(d) and 4(f) suggests that the increasing of λ_L moves each closest pair of ladder rungs (system eigenenergies) apart from each other (see also Fig. 2), thus opening the possibility of new optical transitions in distinct frequencies and, hence, changing the corresponding emission spectrum profile as a function of ω.

In Fig. 5, we particularly analyze the competition of λ_L and Ω_R energy scales in the mutation of the doublet structure, formed very near to $\omega = \omega_c$ in the emission spectrum for $\lambda_L = 0$ [Fig. 4(a)], to a single peak localized at $\omega = \omega_c$ when $\lambda_L \neq 0$ [Figs. 3(e) and 4(e)], considering the same other parameters adopted in Fig. 3.

Figures 5(a) and 5(b) exhibit the emission spectrum as a function of the emitted photon frequency for distinct values of λ_L, in linear and logarithmic scales, respectively, considering the same value of Rabi frequency $\Omega_R = 0.1$ adopted throughout this work. Both panels indicate that the well-resolved doublet structure around $\omega = \omega_c$ for $\lambda_L = 0$ (red line) transforms into an almost single peak, with two peaks merging with each other for $\lambda_L \leqslant \Omega_R$ (green and magenta lines). For the biggest value of λ_L adopted in Figs. 5(a) and 5(b) (blue line), a well-defined single-peak structure is seen at $\omega = \omega_c$ due to

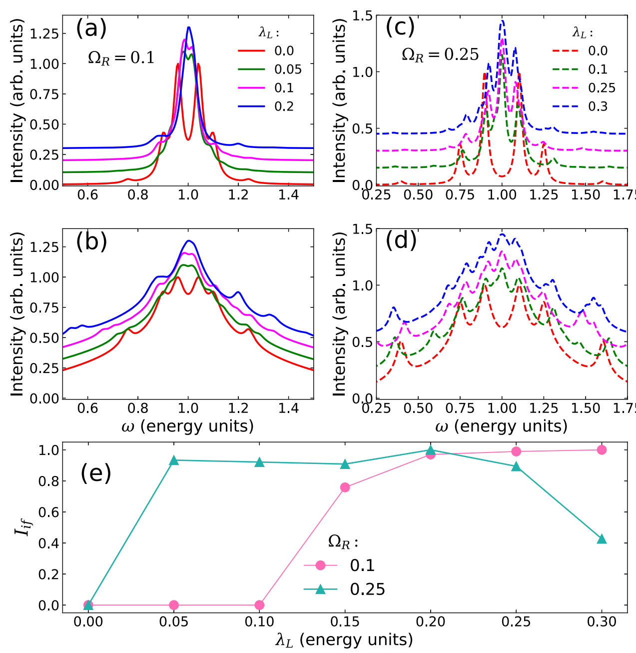

FIG. 5. Top: Normalized emission spectrum [Eq. (10)] as a function of the emitted photon frequency ω, for the situation where the MBSs are well localized at the nanowire ends and do not overlap with each other ($\lambda_R = \varepsilon_M = 0.0$), considering two values of Rabi frequency Ω_R, with $\omega_c = \omega_{eg} = 1.0$, $P = 0.015$, $\gamma_{\text{ph}} = 0.02$, and distinct values of QD–left MBS coupling λ_L. Middle: Same emission spectra of upper panels, but in logarithmic scale. In both top and middle panels, the plots are slightly shifted in the y axis for a better visualization. Bottom: Evolution of the normalized transition probabilities [Eq. (8)] at frequency $\omega \approx \omega_c$ as a function of the QD–left MBS coupling λ_L.

new allowed optical transitions in the system, as discussed earlier. The positions of the satellite peaks also change for distinct values of λ_L, as better visualized in Fig. 5(b).

To investigate if the well-resolved doublet structure around $\omega = \omega_c$ is indeed modified for $\lambda_L \leqslant \Omega_R$, in Figs. 5(c) and 5(d) we consider $\Omega_R = 0.25$. For this value of Rabi frequency, a single peak already arises at ω_c for $\lambda_L < \Omega_R$ (dashed green line) and remains for bigger values of λ_L adopted. The emission spectrum in the logarithmic scale shows a shift in the positions of satellite peaks with λ_L, as also observed in Fig. 5(b).

The findings shown in Figs. 5(a)–5(d) can be explained by Fig. 5(e), which depicts the behavior of the normalized transition probabilities of the system [Eq. (8)] at the cavity eigenfrequency $\omega \approx \omega_c$ as a function of λ_L, for both the values of Ω_R adopted in the upper panels. For $\Omega_R = 0.1$, there is no optical transition allowed at the cavity eigenfrequency when $\lambda_L \leqslant \Omega_R$. This is the reason why we see merging peaks very near $\omega = \omega_c$ instead of a well-defined single peak in Figs. 5(a) and 5(b) when $\lambda_L = 0.05$ and $\lambda_L = 0.1$, although the characteristic well-resolved doublet structure around the cavity eigenfrequency for $\lambda_L = 0$ is suppressed. When the Rabi frequency is increased for $\Omega_R = 0.25$, Fig. 5(e) reveals that $\lambda_L \leqslant \Omega_R$ is enough for allowing optical transitions with frequency on resonance with the cavity eigenfrequency, thus yielding well-defined peaks at $\omega = \omega_c$ in the emission spectrum. Nevertheless, Fig. 5 shows that a small leaking strength of the left MBS into the QD $\lambda_L \leqslant \Omega_R$ spoils the well-resolved emission spectrum doublet structure around $\omega = \omega_c$, leading to either merging peaks or a well-defined single peak at the cavity eigenfrequency, being this last one due to finite transition probabilities at this frequency.

Figure 6(a) exhibits the normalized emission spectrum as a function of the emitted photon frequency ω and the overlap strength ε_M between the MBSs at opposite ends of the nanowire [case (ii)], for $\lambda_L = 0.3$. It is noticed that the increasing of ε_M does not change the single-peak structure at $\omega_c = 1.0$ present in the previous case of isolated MBSs (Fig. 3). The persistent central peak in the presence of a finite MBS-MBS overlap is also shown in the linecuts of Figs. 6(c), 6(e), and 6(g), respectively.

The difference between the current case of finite ε_M and the previous case of isolated MBSs is unveiled in the logarithmic scale, as exhibited in Fig. 6(b) and the corresponding linecuts in Figs. 6(d), 6(f), and 6(h). The emergence is seen of several peaks near each other with very low amplitude, even on a logarithmic scale. These low-amplitude multipeaks arise owing to the opening of new optical transitions caused by the degeneracy breaking of the energy levels due to $\varepsilon_M \neq 0$ [Figs. 2(c) and 2(d)].

The situation [case (iii)] wherein the right MBSs are not well localized at the nanowire end ($\lambda_R \gg \varepsilon_M$) is illustrated in Fig. 7, for $\lambda_L = 0.6$. Figure 7(a) reveals the emission spectrum behavior as a function of both the emitted photon frequency ω and QD–right MBS coupling λ_R. As in the previous case of overlapped MBSs localized at the nanowire ends (Fig. 6), the single-peak structure at the cavity eigenfrequency $\omega_c = 1.0$ still remains, even for higher values of λ_R. The single peak in the emission spectrum also can be seen in the corresponding linecuts shown in Figs. 7(c), 7(e), and 7(g).

The difference between the current case and the previous situations of highly isolated MBSs [Fig. 3(b)] and overlapped MBSs [Fig. 6(b)] is observed in the emitted radiation of low and high frequency, and thus it is only visible on a logarithmic scale, as shown in Fig. 7(b). The most striking difference is the presence of a peak at very low frequency ($\omega \approx 0.1$), as well as a peak near the region of double frequency, precisely at $\omega \approx 1.75$, which remain for all values of λ_R adopted, as depicted in the corresponding linecuts shown in Figs. 7(d), 7(f), and 7(h), respectively. The emitted radiation at very low frequency comes from allowed optical transitions between the nearest energy levels of the corresponding ladder shown in Fig. 2(f), for instance. Oppositely, the emitted radiation in the region around $\omega \approx 1.75$ appears due to transitions between the farthest rungs of the corresponding ladder.

IV. CONCLUSIONS

We have analyzed the optical response of a quantum dot (QD) embedded in a microcavity and coupled to a Majorana nanowire hosting Majorana bound states (MBSs) at its opposite ends. In the regime of strong light-matter coupling, we demonstrated that the coupling between the Majorana nanowire and the QD opens new optical transitions between the polaritonic states of the QD-microcavity system, thus reshaping the well-known JC ladder. Moreover, we also

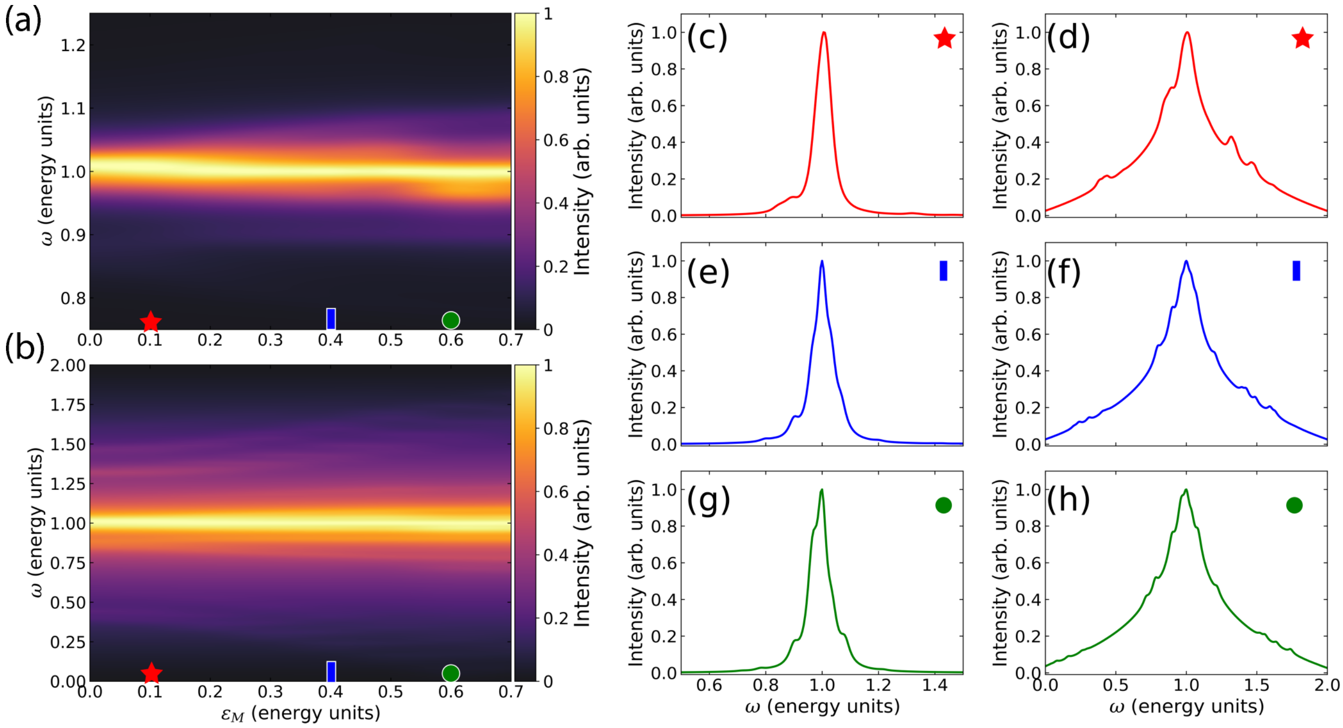

FIG. 6. Normalized emission spectrum [Eq. (10)] for the situation of MBSs localized at opposite nanowire ends ($\lambda_R = 0.0$), but with a finite overlap ε_M between each other, with $\lambda_L = 0.3$, $\omega_c = \omega_{eg} = 1.0$, $\Omega_R = 0.1$, $P = 0.015$, and $\gamma_{\text{ph}} = 0.02$. [(a), (b)] Intensity of emission spectrum as a function of both emitted photon frequency ω and left-right MBS overlap ε_M, in linear and logarithmic scales, respectively. [(c), (e), (g)] Linecuts indicated by geometric shape markers in (a); [(d), (f), (h)] the same linecuts, but in logarithmic scale.

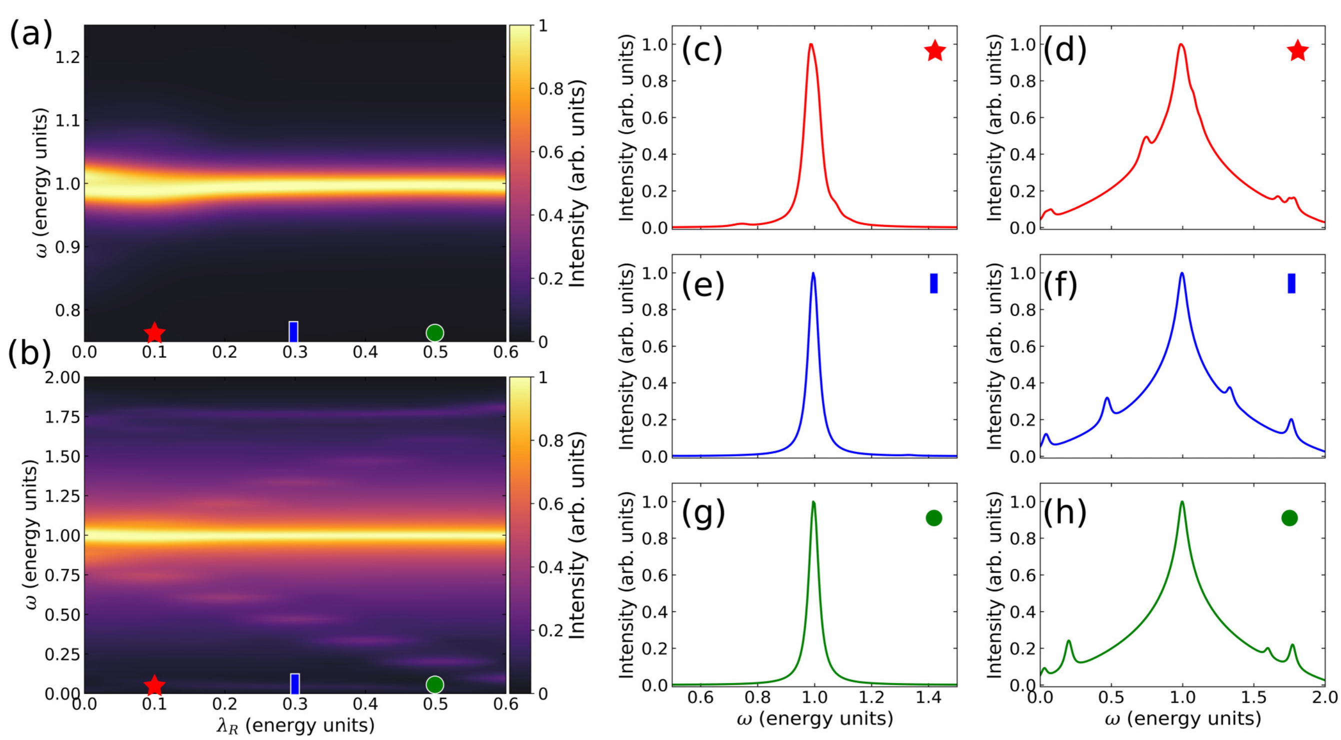

FIG. 7. Normalized emission spectrum [Eq. (10)] for the situation where the MBSs are not well localized at the nanowire ends ($\lambda_R \neq 0.0$) and have a negligible overlap between each other ($\varepsilon_M \ll \lambda_R, \lambda_L$), with $\lambda_L = 0.6$, $\omega_c = \omega_{eg} = 1.0$, $\Omega_R = 0.1$, $P = 0.015$, and $\gamma_{\text{ph}} = 0.02$. [(a), (b)] Intensity of emission spectrum as a function of both emitted photon frequency ω and QD–right MBS coupling λ_R, in linear and logarithmic scales, respectively. [(c), (e), (g)] Linecuts indicated by geometric shape markers in (a); [(d), (f), (h)] the same linecuts, but in logarithmic scale.

demonstrated that the reshaping of the ladder rungs and corresponding optical transitions depend on the spatial location of the MBSs with respect to the nanowire ends, as well as the overlap between them. Consequently, the opening of new transitions strongly affects the cavity emission spectrum, which shows an asymmetric pattern having a prominent single-peak structure centered at the cavity eigenfrequency for all the cases explored, namely, highly isolated MBSs localized at the nanowire ends, overlapped MBSs, and the right MBS displaced from its corresponding nanowire end. The distinction between the three situations is observed only in the emitted radiation of low and high frequency.

ACKNOWLEDGMENTS

This work was supported by the Icelandic Research Fund (project "Hybrid polaritonics"). V.K.K. acknowledges the support from the Georg H. Endress foundation. A.C.S. acknowledges support from Brazilian National Council for Scientific and Technological Development (CNPq), Grants No. 305668/2018-8 and No. 308695/2021-6. I.A.S. acknowledges support from the Ministry of Science and Higher Education of Russian Federation, state assignment No. 2019-1246 and Priority 2030 Federal Academic Leadership Program.

[1] E. Majorana, Teoria simmetrica dell'elettrone e del positrone, Il Nuovo Cimento **14**, 171 (1937).

[2] J. Alicea, New directions in the pursuit of Majorana fermions in solid state systems, Rep. Prog. Phys. **75**, 076501 (2012).

[3] S. R. Elliott and M. Franz, Colloquium, Rev. Mod. Phys. **87**, 137 (2015).

[4] R. Aguado, Majorana quasiparticles in condensed matter, Riv. Nuovo Cimento **40**, 523 (2017).

[5] B. Jäck, Y. Xie, and A. Yazdani, Detecting and distinguishing Majorana zero modes with the scanning tunneling microscope, Nat. Rev. Phys. **3**, 541 (2021).

[6] K. Laubscher and J. Klinovaja, Majorana bound states in semiconducting nanostructures, J. Appl. Phys. **130**, 081101 (2021).

[7] C. Nayak, S. H. Simon, A. Stern, M. Freedman, and S. Das Sarma, Non-Abelian anyons and topological quantum computation, Rev. Mod. Phys. **80**, 1083 (2008).

[8] A. Kitaev, Fault-tolerant quantum computation by anyons, Ann. Phys. **303**, 2 (2003).

[9] D. Aasen, M. Hell, R. V. Mishmash, A. Higginbotham, J. Danon, M. Leijnse, T. S. Jespersen, J. A. Folk, C. M. Marcus, K. Flensberg, and J. Alicea, Milestones Toward Majorana-Based Quantum Computing, Phys. Rev. X **6**, 031016 (2016).

[10] A. Y. Kitaev, Unpaired Majorana fermions in quantum wires, Phys. Usp. **44**, 131 (2001).

[11] R. M. Lutchyn, J. D. Sau, and S. Das Sarma, Majorana Fermions and a Topological Phase Transition in Semiconductor-Superconductor Heterostructures, Phys. Rev. Lett. **105**, 077001 (2010).

[12] Y. Oreg, G. Refael, and F. von Oppen, Helical Liquids and Majorana Bound States in Quantum Wires, Phys. Rev. Lett. **105**, 177002 (2010).

[13] R. M. Lutchyn, E. P. A. M. Bakkers, L. P. Kouwenhoven, P. Krogstrup, C. M. Marcus, and Y. Oreg, Majorana zero modes in superconductor–semiconductor heterostructures, Nat. Rev. Mater. **3**, 52 (2018).

[14] F. Nichele, A. C. C. Drachmann, A. M. Whiticar, E. C. T. O'Farrell, H. J. Suominen, A. Fornieri, T. Wang, G. C. Gardner, C. Thomas, A. T. Hatke, P. Krogstrup, M. J. Manfra, K. Flensberg, and C. M. Marcus, Scaling of Majorana Zero-Bias Conductance Peaks, Phys. Rev. Lett. **119**, 136803 (2017).

[15] V. Mourik, K. Zuo, S. M. Frolov, S. R. Plissard, E. P. A. M. Bakkers, and L. P. Kouwenhoven, Signatures of Majorana fermions in hybrid superconductor-semiconductor nanowire devices, Science **336**, 1003 (2012).

[16] E. Prada, P. San-Jose, and R. Aguado, Transport spectroscopy of *ns* nanowire junctions with majorana fermions, Phys. Rev. B **86**, 180503(R) (2012).

[17] S. M. Albrecht, A. Higginbotham, M. Madsen, F. Kuemmeth, T. S. Jespersen, J. Nygård, P. Krogstrup, and C. Marcus, Exponential protection of zero modes in Majorana islands, Nature (London) **531**, 206 (2016).

[18] P. Krogstrup, N. L. B. Ziino, W. Chang, S. M. Albrecht, M. H. Madsen, E. Johnson, J. Nygård, C. M. Marcus, and T. S. Jespersen, Epitaxy of semiconductor–superconductor nanowires, Nat. Mater. **14**, 400 (2015).

[19] M. T. Deng, S. Vaitiekenas, E. B. Hansen, J. Danon, M. Leijnse, K. Flensberg, J. Nygård, P. Krogstrup, and C. M. Marcus, Majorana bound state in a coupled quantum-dot hybrid-nanowire system, Science **354**, 1557 (2016).

[20] H. Zhang, D. E. Liu, M. Wimmer, and L. P. Kouwenhoven, Quantum transport in Majorana nanowire devices: Next steps, Nat. Commun. **10**, 5128 (2019).

[21] E. Vernek, P. H. Penteado, A. C. Seridonio, and J. C. Egues, Subtle leakage of a Majorana mode into a quantum dot, Phys. Rev. B **89**, 165314 (2014).

[22] M.-T. Deng, S. Vaitiekėnas, E. Prada, P. San-Jose, J. Nygård, P. Krogstrup, R. Aguado, and C. M. Marcus, Nonlocality of Majorana modes in hybrid nanowires, Phys. Rev. B **98**, 085125 (2018).

[23] E. Prada, R. Aguado, and P. San-Jose, Measuring Majorana nonlocality and spin structure with a quantum dot, Phys. Rev. B **96**, 085418 (2017).

[24] F. Peñaranda, R. Aguado, P. San-Jose, and E. Prada, Quantifying wave-function overlaps in inhomogeneous Majorana nanowires, Phys. Rev. B **98**, 235406 (2018).

[25] D. J. Clarke, Experimentally accessible topological quality factor for wires with zero energy modes, Phys. Rev. B **96**, 201109(R) (2017).

[26] L. S. Ricco, Y. Marques, J. E. Sanches, I. A. Shelykh, and A. C. Seridonio, Interaction induced hybridization of Majorana zero modes in a coupled quantum-dot–superconducting-nanowire hybrid system, Phys. Rev. B **102**, 165104 (2020).

[27] L. S. Ricco, J. E. Sanches, Y. Marques, M. de Souza, M. S. Figeura, I. A. Shelykh, and A. C. Seridonio, Topological isoconductance signatures in Majorana nanowires, Sci. Rep. **11**, 17310 (2021).

[28] A. Cottet, T. Kontos, and B. Doucot, Squeezing light with Majorana fermions, Phys. Rev. B **88**, 195415 (2013).

[29] M. Trif and Y. Tserkovnyak, Resonantly Tunable Majorana Polariton in a Microwave Cavity, Phys. Rev. Lett. **109**, 257002 (2012).
[30] M. C. Dartiailh, T. Kontos, B. Douçot, and A. Cottet, Direct Cavity Detection of Majorana Pairs, Phys. Rev. Lett. **118**, 126803 (2017).
[31] H.-Z. Tang, Y.-T. Zhang, and J.-J. Liu, Photon-assisted tunneling through a topological superconductor with Majorana bound states, AIP Adv. **5**, 127129 (2015).
[32] Z. Wang, Q.-F. Liang, D.-X. Yao, and X. Hu, Viewing Majorana bound states by Rabi oscillations, Sci. Rep. **5**, 11686 (2015).
[33] H. J. Chen and H. W. Wu, Rabi splitting and optical Kerr nonlinearity of quantum dot mediated by Majorana fermions, Sci. Rep. **8**, 17677 (2018).
[34] F. Chi, T.-Y. He, J. Wang, Z.-G. Fu, L.-M. Liu, P. Liu, and P. Zhang, Photon-assisted transport through a quantum dot side-coupled to Majorana bound states, Front. Phys. **8**, 254 (2020).
[35] D. M. T. van Zanten, D. Sabonis, J. Suter, J. I. Väyrynen, T. Karzig, D. I. Pikulin, E. C. T. O'Farrell, D. Razmadze, K. D. Petersson, P. Krogstrup, and C. M. Marcus, Photon-assisted tunnelling of zero modes in a Majorana wire, Nat. Phys. **16**, 663 (2020).
[36] C. Peng, A. Haim, T. Karzig, Y. Peng, and G. Refael, Floquet Majorana bound states in voltage-biased planar Josephson junctions, Phys. Rev. Research **3**, 023108 (2021).
[37] L. S. Ricco, V. K. Kozin, A. C. Seridonio, and I. A. Shelykh, Accessing the degree of Majorana nonlocality in a quantum dot-optical microcavity system, Sci. Rep. **12**, 1983 (2022).
[38] L. C. Contamin, M. R. Delbecq, B. D. Çot, A. Cottet, and T. Kontos, Hybrid light-matter networks of Majorana zero modes, arXiv:2103.16679
[39] L. Bittermann, C. D. Beule, D. Frombach, and P. Recher, Probing Majorana bound states via a pn-junction containing a quantum dot, arXiv:2112.11862.
[40] P. Senellart, G. Solomon, and A. White, High-performance semiconductor quantum-dot single-photon sources, Nat. Nanotechnol. **12**, 1026 (2017).
[41] O. Benson, C. Santori, M. Pelton, and Y. Yamamoto, Regulated and Entangled Photons from a Single Quantum Dot, Phys. Rev. Lett. **84**, 2513 (2000).
[42] R. Johne, N. A. Gippius, G. Pavlovic, D. D. Solnyshkov, I. A. Shelykh, and G. Malpuech, Entangled Photon Pairs Produced by a Quantum Dot Strongly Coupled to a Microcavity, Phys. Rev. Lett. **100**, 240404 (2008).
[43] M. Peiris, K. Konthasinghe, and A. Muller, Franson Interference Generated by a Two-Level System, Phys. Rev. Lett. **118**, 030501 (2017).
[44] C. H. H. Schulte, J. Hansom, A. E. Jones, C. Matthiesen, C. Le Gall, and M. Atature, Quadrature squeezed photons from a two-level system, Nature (London) **525**, 222 (2008).
[45] R. Trivedi, K. A. Fischer, J. Vučković, and K. Müller, Generation of non-classical light using semiconductor quantum dots, Adv. Quantum Technol. **3**, 1900007 (2020).
[46] Q. Bin, X.-Y. Lü, F. P. Laussy, F. Nori, and Y. Wu, n-Phonon Bundle Emission via the Stokes Process, Phys. Rev. Lett. **124**, 053601 (2020).
[47] A. Ridolfo, O. Di Stefano, N. Fina, R. Saija, and S. Savasta, Quantum Plasmonics with Quantum Dot-Metal Nanoparticle Molecules: Influence of the Fano Effect on Photon Statistics, Phys. Rev. Lett. **105**, 263601 (2010).
[48] K. A. Fischer, Y. A. Kelaita, N. V. Sapra, C. Dory, K. G. Lagoudakis, K. Müller, and J. Vučković, On-Chip Architecture for Self-Homodyned Nonclassical Light, Phys. Rev. Applied **7**, 044002 (2017).
[49] A. P. Foster, D. Hallett, I. V. Iorsh, S. J. Sheldon, M. R. Godsland, B. Royall, E. Clarke, I. A. Shelykh, A. M. Fox, M. S. Skolnick, I. E. Itskevich, and L. R. Wilson, Tunable Photon Statistics Exploiting the Fano Effect in a Waveguide, Phys. Rev. Lett. **122**, 173603 (2019).
[50] M. Arcari, I. Söllner, A. Javadi, S. Lindskov Hansen, S. Mahmoodian, J. Liu, H. Thyrrestrup, E. H. Lee, J. D. Song, S. Stobbe, and P. Lodahl, Near-Unity Coupling Efficiency of a Quantum Emitter to a Photonic Crystal Waveguide, Phys. Rev. Lett. **113**, 093603 (2014).
[51] P. Lodahl, S. Mahmoodian, and S. Stobbe, Interfacing single photons and single quantum dots with photonic nanostructures, Rev. Mod. Phys. **87**, 347 (2015).
[52] C. P. Dietrich, A. Fiore, M. G. Thompson, M. Kamp, and S. Höfling, GaAs integrated quantum photonics: Towards compact and multi-functional quantum photonic integrated circuits, Laser Photonics Rev. **10**, 870 (2016).
[53] T. Yoshie, A. Scherer, J. Hendrickson, G. Khitrova, H. M. Gibbs, G. Rupper, C. Ell, O. B. Shchekin, and D. G. Deppe, Vacuum Rabi splitting with a single quantum dot in a photonic crystal nanocavity, Nature (London) **432**, 200 (2004).
[54] J. P. Reithmaier, G. Sek, A. Löffler, C. Hofmann, S. Kuhn, S. Reitzenstein, L. V. Keldysh, V. D. Kulakovskii, T. L. Reinecke, and A. Forchel, Strong coupling in a single quantum dot-semiconductor microcavity system, Nature (London) **432**, 197 (2004).
[55] D. Englund, A. Faraon, I. Fushman, N. Stoltz, P. Petroff, and J. Vučković, Controlling cavity reflectivity with a single quantum dot, Nature (London) **450**, 857 (2007).
[56] E. Jaynes and F. Cummings, Comparison of quantum and semi-classical radiation theories with application to the beam maser, Proc. IEEE **51**, 89 (1963).
[57] B. W. Shore and P. L. Knight, The Jaynes-Cummings Model, J. Mod. Opt. **40**, 1195 (1993).
[58] F. P. Laussy, E. del Valle, M. Schrapp, A. Laucht, and J. J. Finley, Climbing the Jaynes-Cummings ladder by photon counting, J. Nanophotonics **6**, 061803 (2012).
[59] B. R. Mollow, Power spectrum of light scattered by two-level systems, Phys. Rev. **188**, 1969 (1969).
[60] E. del Valle and F. P. Laussy, Regimes of strong light-matter coupling under incoherent excitation, Phys. Rev. A **84**, 043816 (2011).
[61] K. A. Fischer, K. Müller, A. Rundquist, T. Sarmiento, A. Y. Piggott, Y. Kelaita, C. Dory, K. G. Lagoudakis, and J. Vučković, Self-homodyne measurement of a dynamic Mollow triplet in the solid state, Nat. Photonics **10**, 163 (2016).
[62] J. C. L. Carreño, C. Sánchez Muñoz, E. del Valle, and F. P. Laussy, Excitation with quantum light. II. Exciting a two-level system, Phys. Rev. A **94**, 063826 (2016).
[63] O. V. Kibis, G. Y. Slepyan, S. A. Maksimenko, and A. Hoffmann, Matter Coupling to Strong Electromagnetic Fields in Two-Level Quantum Systems with Broken Inversion Symmetry, Phys. Rev. Lett. **102**, 023601 (2009).
[64] I. G. Savenko, O. V. Kibis, and I. A. Shelykh, Asymmetric quantum dot in a microcavity as a nonlinear optical element, Phys. Rev. A **85**, 053818 (2012).

[65] F. P. Laussy, M. M. Glazov, A. Kavokin, D. M. Whittaker, and G. Malpuech, Statistics of excitons in quantum dots and their effect on the optical emission spectra of microcavities, Phys. Rev. B **73**, 115343 (2006).

[66] E. del Valle, F. P. Laussy, F. M. Souza, and I. A. Shelykh, Optical spectra of a quantum dot in a microcavity in the nonlinear regime, Phys. Rev. B **78**, 085304 (2008).

[67] D. E. Liu and H. U. Baranger, Detecting a Majorana-fermion zero mode using a quantum dot, Phys. Rev. B **84**, 201308(R) (2011).

[68] H. Pan, C.-X. Liu, M. Wimmer, and S. Das Sarma, Quantized and unquantized zero-bias tunneling conductance peaks in Majorana nanowires: Conductance below and above $2e^2/h$, Phys. Rev. B **103**, 214502 (2021).

[69] H. Pan and S. Das Sarma, Disorder effects on Majorana zero modes: Kitaev chain versus semiconductor nanowire, Phys. Rev. B **103**, 224505 (2021).

[70] E. Prada, P. San-Jose, M. W. A. de Moor, A. Geresdi, E. J. H. Lee, J. Klinovaja, D. Loss, J. Nygård, R. Aguado, and L. P. Kouwenhoven, From Andreev to Majorana bound states in hybrid superconductor-semiconductor nanowires, Nat. Rev. Phys. **2**, 575 (2020).

[71] A. Vuik, B. Nijholt, A. R. Akhmerov, and M. Wimmer, Reproducing topological properties with quasi-Majorana states, SciPost Phys. **7**, 061 (2019).

[72] L. S. Ricco, V. L. Campo, I. A. Shelykh, and A. C. Seridonio, Majorana oscillations modulated by Fano interference and degree of nonlocality in a topological superconducting-nanowire–quantum-dot system, Phys. Rev. B **98**, 075142 (2018).

[73] L. S. Ricco, M. de Souza, M. S. Figueira, I. A. Shelykh, and A. C. Seridonio, Spin-dependent zero-bias peak in a hybrid nanowire-quantum dot system: Distinguishing isolated Majorana fermions from Andreev bound states, Phys. Rev. B **99**, 155159 (2019).

[74] A. V. Kavokin, J. J. Baumberg, G. Malpuech, and F. P. Laussy, *Microcavities*, On Semiconductor Science and Technology (Oxford University Press, Oxford, UK, 2017).

[75] J. Johansson, P. Nation, and F. Nori, QuTiP: An open-source Python framework for the dynamics of open quantum systems, Comput. Phys. Commun. **183**, 1760 (2012).

[76] J. Johansson, P. Nation, and F. Nori, QuTiP 2: A Python framework for the dynamics of open quantum systems, Comput. Phys. Commun. **184**, 1234 (2013).

[77] E. del Valle, F. P. Laussy, and C. Tejedor, Luminescence spectra of quantum dots in microcavities. II. Fermions, Phys. Rev. B **79**, 235326 (2009).

[78] Y. Todorov, I. Sagnes, I. Abram, and C. Minot, Purcell Enhancement of Spontaneous Emission from Quantum Cascades Inside Mirror-Grating Metal Cavities at THz Frequencies, Phys. Rev. Lett. **99**, 223603 (2007).

[79] F. Sizov and A. Rogalski, THz detectors, Prog. Quantum Electron. **34**, 278 (2010).